READ 2024
RESEARCH & EDUCATION IN AIRCRAFT DESIGN
WARSAW, POLAND | 6-8 NOVEMBER 2024

OPTIMIZATION OF THE UNMANNED AERIAL VEHICLE WING PLANFORM TO MAXIMIZE FLIGHT ENDURANCE

Justyna Pluta[1]

[1]Warsaw University of Technology, the Faculty of Power and Aerospace Engineering

Abstract

This work presents a comprehensive approach to optimizing the wing planform of an unmanned aerial vehicle (UAV) in a flying wing configuration, with the objective of maximizing flight endurance. The study focuses on the aerodynamic design process and its optimization, integrating various multidisciplinary elements to address both the challenges and potential solutions in UAV performance.

Keywords: optimization, flight endurance, UAVs, genetic algorithms

1. Motivation and Research Context

Unmanned Aerial Vehicles (UAVs) are a rapidly developing, multidisciplinary area of science, driven by their flexibility and wide range of applications. The ability to equip UAVs with various sensors and specialized tools enables their use in fields such as surveillance, agriculture, and mapping. This versatility has sparked widespread interest, motivating a focus on this type of unmanned system. This work aims to improve UAV performance through optimization techniques, addressing challenges related to flight endurance and efficiency, which are essential for advancing UAV technology.

1.1 UAVs classification and trend analysis

A trend analysis of current configurations was conducted, providing a foundation for examining the main issues and challenges UAVs face today. UAVs are diverse and can be classified in various ways due to their different designs and applications. The main classification categories include: type of aircraft, weight class, propulsion type, operational range and altiude.

Type	MTOW	Example
Nano	$<$200 g	PD-100 Black Hornet III
Micro	$<$5 kg	Dragon Eye
Light	5-50 kg	Silver Fox
Middle	50-200 kg	Lemur
Heavy	200-2000 kg	PGZ-19R Orlik
Super heavy	$>$2000 kg	Predator B

Table 1 – UAVs classification by weight [1].

The search area was narrowed to micro UAVs, for which a flight endurance analysis was performed. Conclusions from the trend analysis indicate that UAVs in the under-5 kg category are primarily powered by electric engines, which are well-suited for reconnaissance missions due to their quiet operation. However, for flights requiring endurance beyond several hours, transitioning to combustion engines becomes necessary. An example of this is the BirdEye UAV, as shown in Figure 1, which achieves a flight endurance of up to 15 hours with a combustion engine.

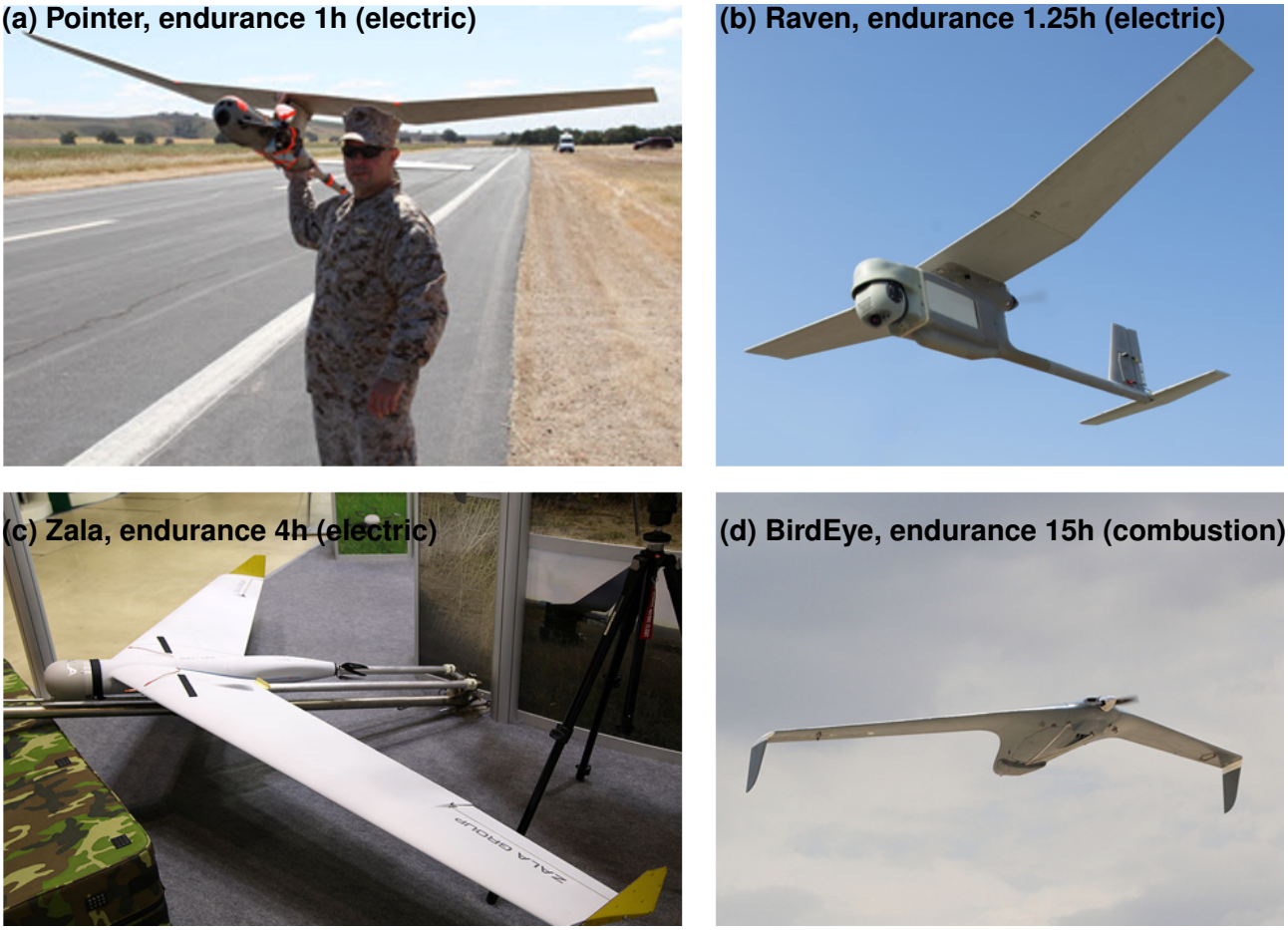

Figure 1 – Comparison of micro drones by endurance and propulsion. (a) Pointer[2] (b) Raven[3] (c) Zala[4] (d) BirdEye[5].

The trend analysis highlights that the limited flight endurance of micro UAVs is primarily due to the reliance on electric engines and the low energy density of current power sources. To address this, optimization efforts are needed to enhance performance, with a focus on improving aerodynamic efficiency while working within the constraints of existing power source technology.

2. Assumptions and approach

The development of the optimization model began by defining the optimization criteria and identifying basic aerodynamic and mass-related dependencies.

2.1 Flight endurance equation

Initial flight endurance t for an electrically powered UAV was estimated using a formula that depends on the power requirement for level flight at cruise speed V_c. Here, E represents the energy capacity of the battery, influenced by cell count, capacity, voltage, and efficiency η.
From the equilibrium condition, where lift equals the aircraft's weight ($L = W$) and thrust equals aerodynamic drag ($T = D$), the necessary power is determined as the product of drag and cruise speed. This relationship forms the basis for calculating the power requirements for level, steady flight and is fundamental to optimizing the UAV's endurance based on battery capacity and aerodynamic efficiency.

$$t = \frac{E}{D \cdot V_c} = \frac{V_{\text{cell}} \cdot \text{number of cells} \cdot Q_{\text{cell}} \cdot \eta_{\text{cell}}}{\frac{1}{2}\rho V_c^3 \cdot S \cdot C_D} \quad [h] \tag{1}$$

These initial calculations provide a simplified framework for determining the key parameters impacting flight endurance, setting the stage for optimization by minimizing C_D and maximizing E within design constraints. Further stages will involve developing a detailed model that incorporates these foundational equations alongside additional aerodynamic and structural considerations.

2.2 Initial configuration

Before building the optimization model, basic assumptions and the UAV's mission profile were established. The project focuses on designing a micro UAV powered by a quiet electric motor, with a compact design capable of hand launch. The UAV is intended primarily for surveillance and patrol operations, with a maximum altitude of 120 meters in compliance with EASA regulations for the "Open" category [6].

A preliminary analysis, based on a comparison of minimum drag coefficients, led to the selection of a flying wing configuration due to its aerodynamic efficiency, which is essential for improving flight endurance [7]. Although this configuration provides lower drag, it presents challenges in stability and control, particularly in ensuring proper longitudinal and directional stability without separate tail components. To address these factors, the project includes optimizing both the wing shape and mass distribution to achieve an aerodynamically streamlined structure and sufficient stability level. At this stage, the minimum and cruise speeds of the UAV were also determined based on a simple experiment involving a series of weighted throws and data readings from accelerometers using the Phyphox app [8], as well as trend analysis. The minimum speed was set at $8\,\mathrm{m/s}$, with a cruise speed of $12\,\mathrm{m/s}$. The preliminary design concluded with the selection of the flying wing configuration for the UAV. At this stage, the Skywalker X8 model [9] was chosen as a reference and serves as the foundation for developing the geometric, mass, and aerodynamic optimization models. Decision variables for the optimization program were also established at this stage:

- wingspan b
- aspect ratio AR
- taper ratio TR
- sweep angle Λ
- battery capacity E

3. Optimization program

The optimization program was developed with inspiration from Multidisciplinary Design Optimization (MDO), which integrates various fields to achieve balanced performance improvements across multiple disciplines [10]. This approach provided the foundation for creating a UAV optimization program that considers aerodynamic, structural, and energy-related aspects in parallel.

3.1 Program structure

The optimization program was designed in MATLAB [11], incorporating an aerodynamic analysis tool AVL [12] and a genetic algorithm [13] as the optimization engine. By structuring the program around the chosen decision variables, the tool can evaluate numerous configurations. Each iteration adjusts these parameters to improve endurance while respecting structural limits and aerodynamic efficiency. The optimization program's workflow is divided into three main areas what is depicted on Figure 2.

- Model Setup and Variables: Built in MATLAB with the AVL tool for aerodynamic analysis, the program adjusts wing parameters and battery energy to optimize UAV endurance. Each configuration generates a geometric and mass model.
- Aerodynamic Simulation: Files are sent to the AVL solver to simulate level flight at a cruise speed and with zero pitching moment. Aerodynamic results are returned to MATLAB for calculating drag and endurance.
- Optimization Constraints: Constraints via penalty functions ensure realistic configurations, including stability and positive drag, while excluding non-physical solutions. The genetic algorithm iteratively refines configurations to balance endurance and aerodynamic efficiency.

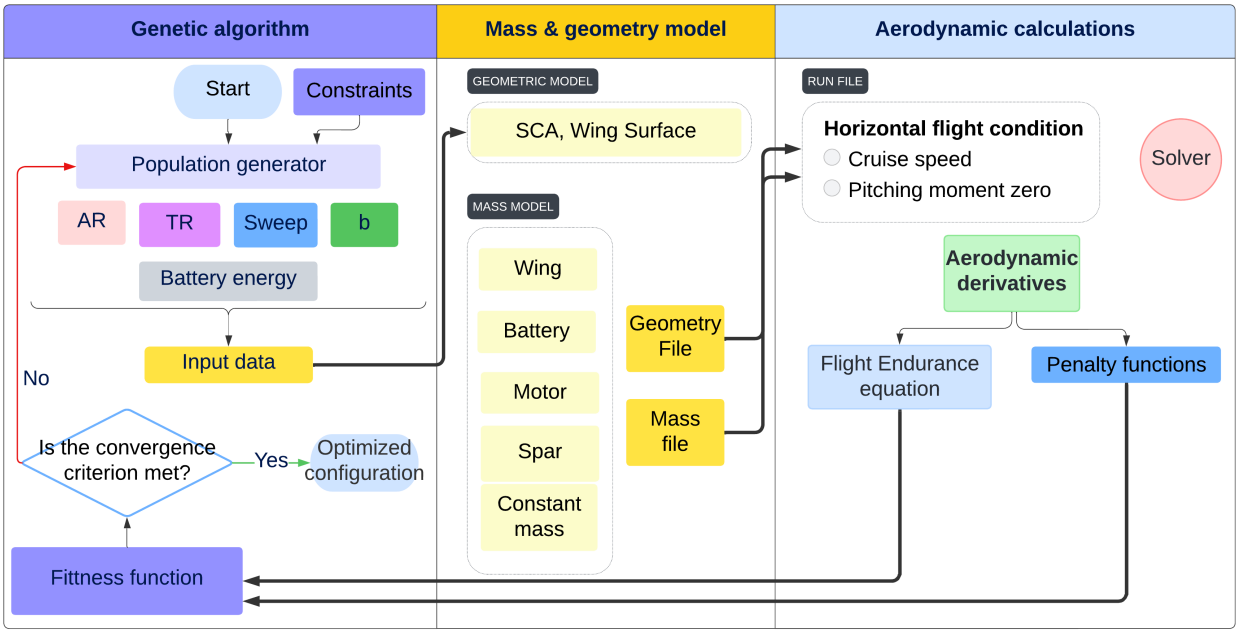

Figure 2 – Optimization program flow.

3.2 Mass model

The mass model is divided into several key components, each represented with specific equations to capture weight distribution and its impact on UAV performance:

$$m_{\textbf{constant}} = 0.279\,\text{kg} \tag{2}$$

Constant Mass: This includes essential onboard components for control and communication, such as servomechanisms, flight controllers, cameras, and auxiliary batteries.

$$m_{\textbf{battery}} = 0.006 \cdot E + 0.053\,\text{kg} \tag{3}$$

Battery Mass: Battery weight depends on energy capacity, modeled based on the trend analysis of available batteries, where E is computed as the product of voltage, cell count, and cell capacity.

$$m_{\text{motor}} = 0.008 \cdot \text{thrust}_{\text{static}} - 0.019\,\text{kg} \tag{4}$$

Motor Mass: Based on motor thrust, the mass is derived from a linear relationship with static thrust values obtained through trend analysis.

$$m_{\text{wing}} = 0.76 \cdot S\,\text{kg} \tag{5}$$

Wing Structure Mass: Calculated from the wing surface area S with a shell structure of composite materials.
Spar Mass: Spar weight depends on the bending moment derived from aerodynamic loading (using Schrenk's method). The overall center of gravity (CG) of the UAV is calculated as a weighted average of each component's CG:

$$X_{\text{CG}} = \frac{\sum(X_{\text{CG}_i} \cdot m_i)}{m_{\text{UAV}}} \tag{6}$$

where X_{CG_i} represents the position of each component's center of gravity and m_i is its mass.
The components with fixed positions are represented as a percentage of the root chord length (c_r).

$$X_{\text{CG, electronics}} = 0.5 \cdot c_r \tag{7}$$

$$X_{\text{CG, motor}} = 1.1 \cdot c_r \tag{8}$$

$$X_{\text{CG, battery}} = 0.0 \cdot c_r \tag{9}$$

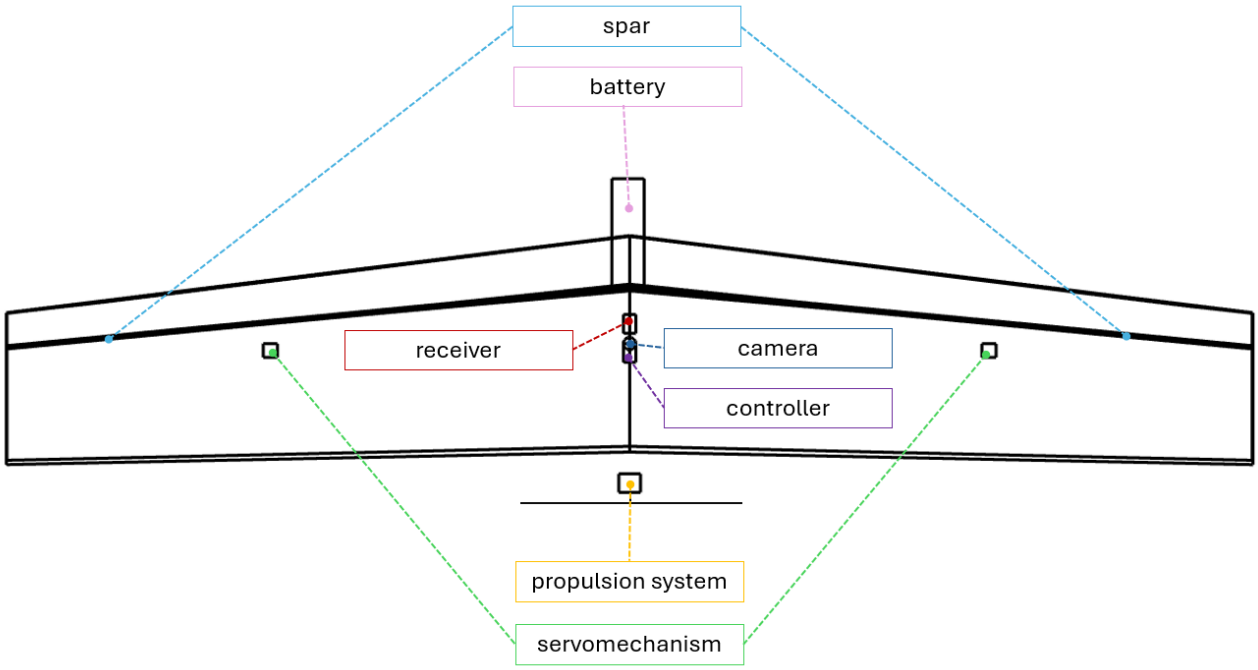

Figure 3 – Mass distribution in the wing.

4. Aerodynamic model

The aerodynamic model is divided into several key aspects to enhance the UAV's performance, focusing on stability, drag reduction, and efficient lift generation.

4.1 Pitch-up phenomenon

The pitch-up phenomenon occurs in swept-wing aircraft, where the nose of the aircraft unexpectedly rises at high angles of attack. This effect is especially pronounced in tailless configurations, like a flying wing, and can lead to instability if not properly managed. To mitigate this, the model limits the aspect ratio (AR) between 6 and 12 and the wing sweep angle (Λ) to a maximum of 15 degrees. These limitations were implemented based on a stability region chart, illustrating areas of stability and instability in terms of pitch-up 4.

4.2 Airfoil selection

The airfoil selection was based on a comparison of aerodynamic characteristics performed in XFOIL [15] for a previously calculated average Reynolds number of 100,000. This analysis led to the choice of the S5020 airfoil [16], known for its low pitching moment coefficient $C_{m_{SA}} = -0.03$, making it suitable for stability in a tailless configuration. With the airfoil selected, the maximum lift coefficient $C_{L_{\text{max}}}$ of the wing was estimated to be 0.8, taking into account the sweep angle [17] and the losses associated with counteracting the pitch moment [14].

4.3 Pitch moment control

In a tailless flying wing, level flight pitch control is achieved through upward deflection of control surfaces, such as elevons. This deflection counteracts the inherent nose-down pitching moment, balancing the aircraft without the need for a traditional tail stabilizer. By adjusting the camber locally, the elevons generate a compensating pitching moment to keep the aircraft stable at cruise.

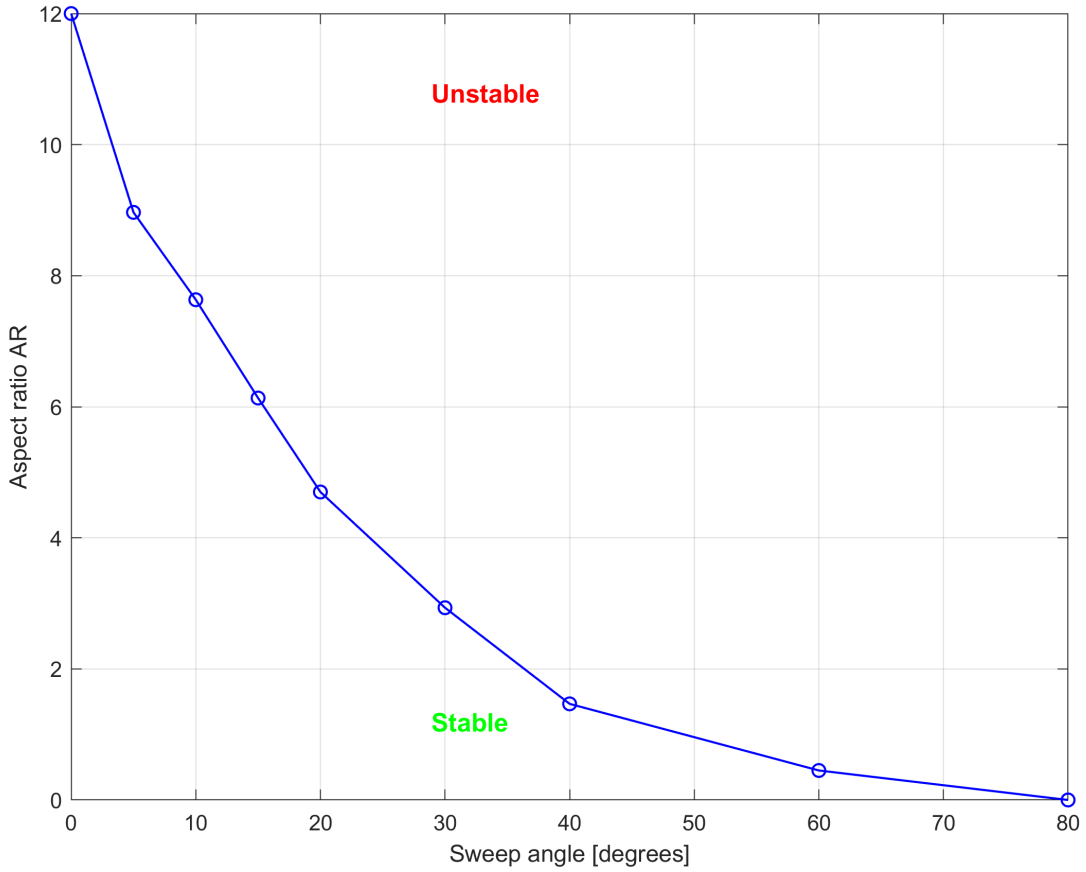

Figure 4 – Pitch-up boundary [14].

For this study, control surface deflection was selected for pitch control due to ease of implementation in the AVL simulation software. Although aerodynamic or geometric wing twist is commonly used for pitch stability in practical applications, deflection allows for dynamic adjustments without altering the fixed wing geometry. This approach provides effective pitch balance in level flight while simplifying the optimization model.

4.4 Drag coefficient

The individual components of the drag coefficient were calculated according to the scheme shown in the figure 5. Induced drag for each aircraft configuration was obtained directly from the AVL program. Due to the use of potential flow models for calculations, it was necessary to estimate the zero-lift drag coefficient C_{D_0} 10 and drag from elevons deflection and drag due to battery fairing separately using analytical methods outside of the AVL program e.g. component buildup method [17]. This combination of methods allowed for a comprehensive assessment of drag components that AVL alone could not capture.

$$C_{D_0} = \frac{\sum(C_f \cdot FF \cdot Q \cdot S_{\text{wet}})}{S_{\text{ref}}} + C_{D_{\text{misc}}} \tag{10}$$

5. Genetic algorithm

Optimization of complex design problems requires effective tools and techniques. This project employs a genetic algorithm (GA), well-suited for optimizing functions of multiple variables in complex, nonlinear solution spaces. Unlike analytical or gradient-based methods, the GA is less likely to get trapped in local optima. By utilizing genetic-inspired mechanisms such as selection, mutation, and crossover, GAs effectively explore even challenging solution spaces.

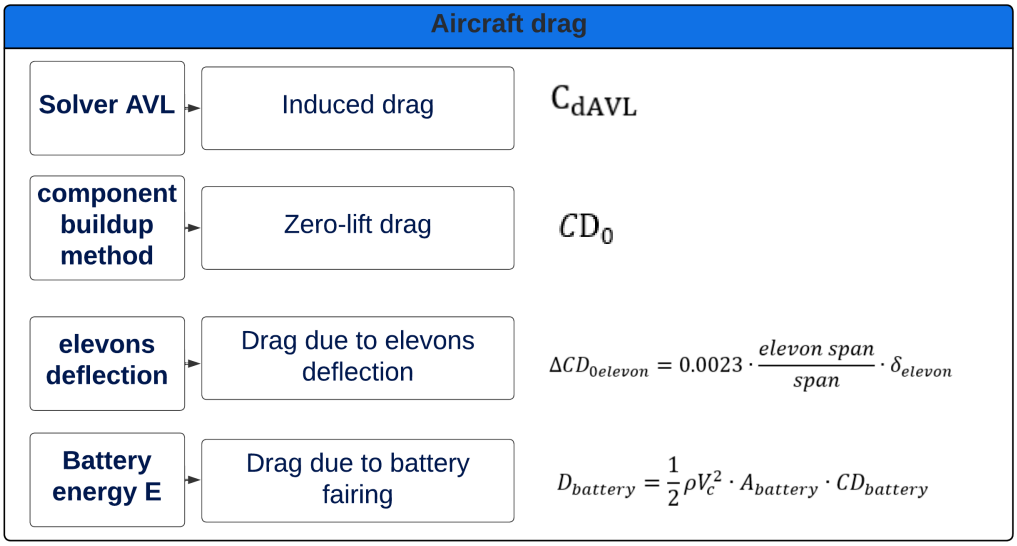

Figure 5 – Aircarft drag calculation summary [14].

This project implements the Genetic Toolbox in MATLAB [13], allowing for straightforward problem definition and parameter tuning of the optimizer. The optimization process follows three main steps:

- **Initial Population Creation**: The algorithm begins by generating an initial population with random parameters, selected from predefined ranges for design variables.
- **Fitness Function**: A fitness function is calculated for each individual, scaled to guide the selection of parent pairs. This scaling prevents dominance by either the strongest or weakest individuals.
- **Offspring Creation**: The next population is generated through three methods: crossover (mixing genes from two parents), mutation (random gene alteration in non-selected individuals), and elite selection (carrying forward the best configurations from the previous generation).

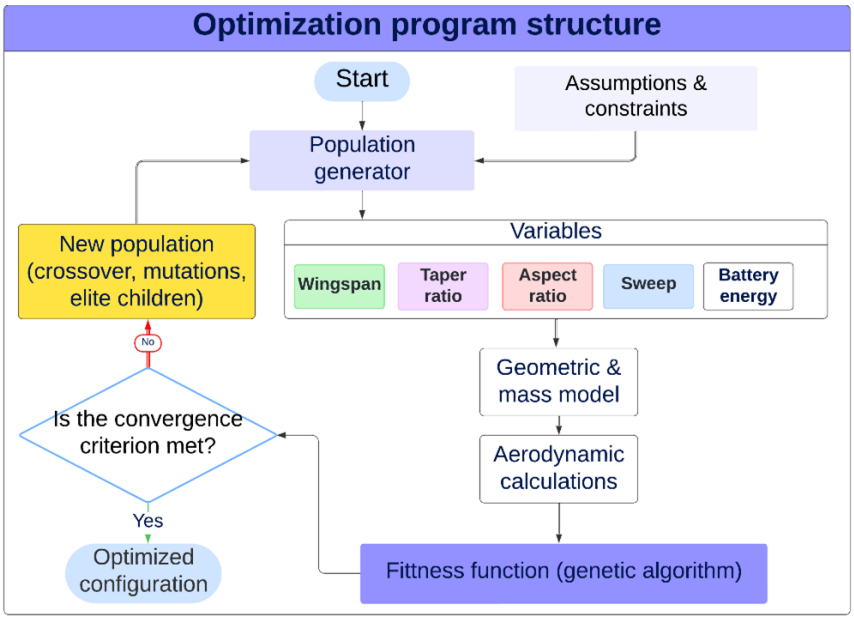

Figure 6 – Genetic algorithm loop structure.

6. Optimization criteria

The optimization assumes that flight endurance primarily depends on cruise drag, as cruise efficiency directly impacts overall endurance. For the climb phase, which is energy-intensive but at the same time short phase, a loss factor of 5% is estimated [18].The objective function is defined as the inverse of endurance:

$$F_{\text{objective}} = \frac{1}{t} \tag{11}$$

The optimization process also includes penalty functions to guide the algorithm by enforcing physical constraints:

- Penalty for Negative Drag Values: Eliminates non-physical configurations by penalizing those with unrealistic (negative) drag values.
- Penalty for Stability Margin Compliance: Rewards configurations that maintain a stability margin between 7% and 12% of the Mean Aerodynamic Chord (MAC), balancing adequate longitudinal stability with maneuverability.
- Penalty for Directional Stability: Discards configurations with negative directional stability derivative C_{n_β}, ensuring stable yaw behavior.
- Penalty for Exceeding Maximum Lift Coefficient: Configurations exceeding the lift threshold $C_{L_{\text{max}}} = 0.8$ are penalized, while those close to it are encouraged to fully utilize aerodynamic potential.

The GA parameters and stopping criteria used to solve the optimization problem:

- Population Size: Increased from the standard 50 to 100 individuals per generation, allowing the algorithm to explore a larger number of configurations each cycle, although this extends calculation time.
- Mutation: A Gaussian mutation was applied, with mutation rates adjusted throughout the optimization. Early generations have a higher mutation rate to explore options broadly, while later generations see reduced rates to focus on refining solutions.
- Elite Count: The top 5% of best-performing individuals are carried over to the next generation unchanged, which supports algorithm stability but is kept limited to avoid early convergence.
- Parent Selection: Roulette selection was chosen over tournament selection, as it favors high-performing candidates while still allowing all individuals a chance to be chosen, which helps maintain variety.
- Maximum Generations: Set to a limit of 100 generations as a stopping point for the algorithm.
- Objective Function Tolerance: A tolerance of 0.001 was set, meaning the optimization stops if improvements between generations fall below this threshold, indicating convergence.

7. Results

The optimization calculations were completed after exploring over five thousand different configurations. The entire process took approximately 1.5 hours and was conducted on a local workstation.

7.1 Optimization summary

The comparison between parameters of the initial and optimized configurations was presented in table 2. Both wing geometry and battery size were adjusted during optimization. The wingspan remained the same, indicating an effort to maximize the use of the available structure. The aspect ratio increased slightly, reducing induced drag while maintaining a large wing area. The battery size was reduced by approximately 20%, yet this adjustment extended flight time from 5 to 6 hours and 20 minutes. The smaller battery also allowed for a reduced cargo compartment size, decreasing fairing drag by 40%. Stability margins were maintained at 7.6%, with the same sweep angle, and elevon

deflection was reduced from -8.44° to -3.8°, further improving aerodynamic efficiency and reducing drag.

Decision variables	Symbol	Initial configuration	Optimized configuration
Span	b	2	1.96
Aspect ratio	AR	6	6.63
Taper ratio	TR	0.4	0.7
Sweep	Λ	3	3
Battery energy	E	185	150
Elevon deflection	δ	-8.43	-3.8
Aircraft drag	D	1.8	1.17
Endurance	t	5 hours 5 minutes	6 hours 20 minutes

Table 2 – Configuration comparision (before and after optimization).

Munk's theorem [19] serves as a useful measure for comparing the aerodynamic efficiency of the initial and optimized configurations. The chart below shows the K_v coefficient across different flight speeds for both configurations. The optimized configuration closely approaches the theoretical value for induced drag (near 1), with only minor losses of a few percent. In contrast, the unoptimized configuration shows induced drag losses of up to 40%, highlighting the significant efficiency gains achieved through optimization.

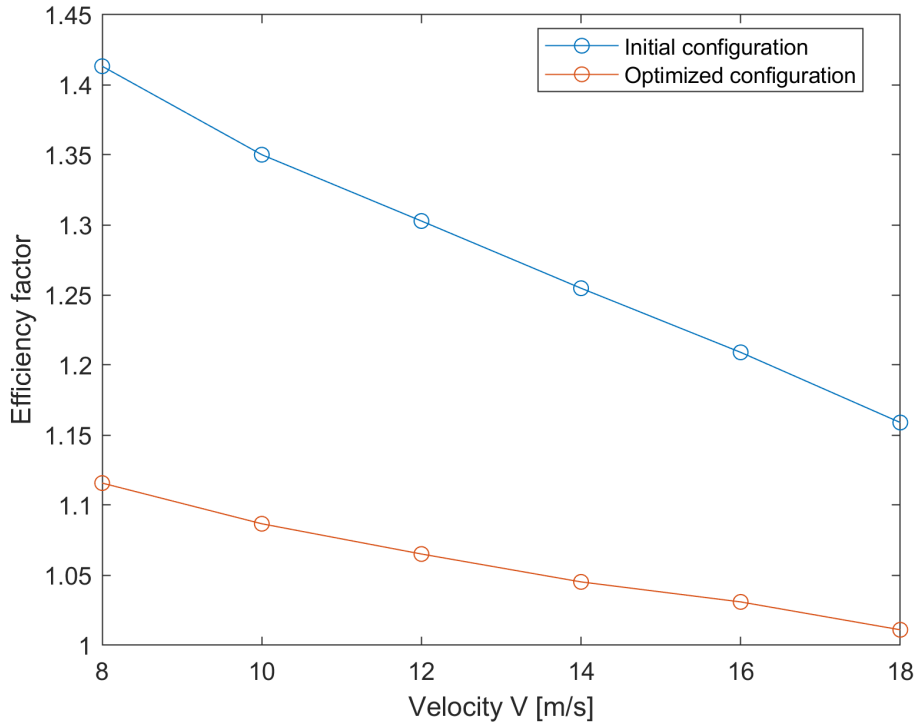

Figure 7 – Efficiency factor of initail and optimized configuration.

7.2 Dynamic stability

As an extension of the project, an additional dynamic stability analysis was conducted for the optimized aircraft configuration. Calculations were performed in the SDSA environment [20], with the aerodynamic grid and derivatives prepared in PANUKL [21]. Mass distribution, based on optimization results, plays a key role in dynamic assessment. Using a parametric wing model in CAD software (NX

Siemens) [22], precise moments of inertia were calculated. The dynamic analysis in SDSA indicated the following results:

- Phugoid Oscillation: Positive stability margin across all speeds, meeting ICAO criteria [23].
- Short-Period Oscillation: Positive stability margin across all speeds, meeting ICAO criteria.
- Roll: Highest first-level stability across all speeds, meeting MIL-F-8785C Phase A criteria [24].
- Dutch Roll: Criterion not met at any speed, based on CS-23 standards [25].
- Spiral Stability: Criterion not met only at low speeds, according to MIL-F-8785C Phase A criteria.

Based on the results, which showed non-compliance with the Dutch roll criterion and partial compliance with spiral stability, steps were taken to address these issues. Improving Dutch roll stability can be achieved by adding vertical surfaces, while enhancing spiral stability requires wing dihedral. However, increased dihedral can negatively impact Dutch roll stability, which is considered more critical. Therefore, the redesign focused primarily on improving Dutch roll characteristics. The process was conducted iteratively, adjusting wing geometry (dihedral and vertical surfaces) and observing dynamic response results in SDSA. In each iteration, the aircraft mass and moments of inertia were updated. A summary of this process is shown in Figure 10.
The result of the dynamic optimization is a configuration that meets the Dutch roll criterion across the entire speed range, with the spiral criterion unmet only at low speeds, below 9 m/s. This is considered acceptable, as Dutch roll poses a significantly higher safety risk.

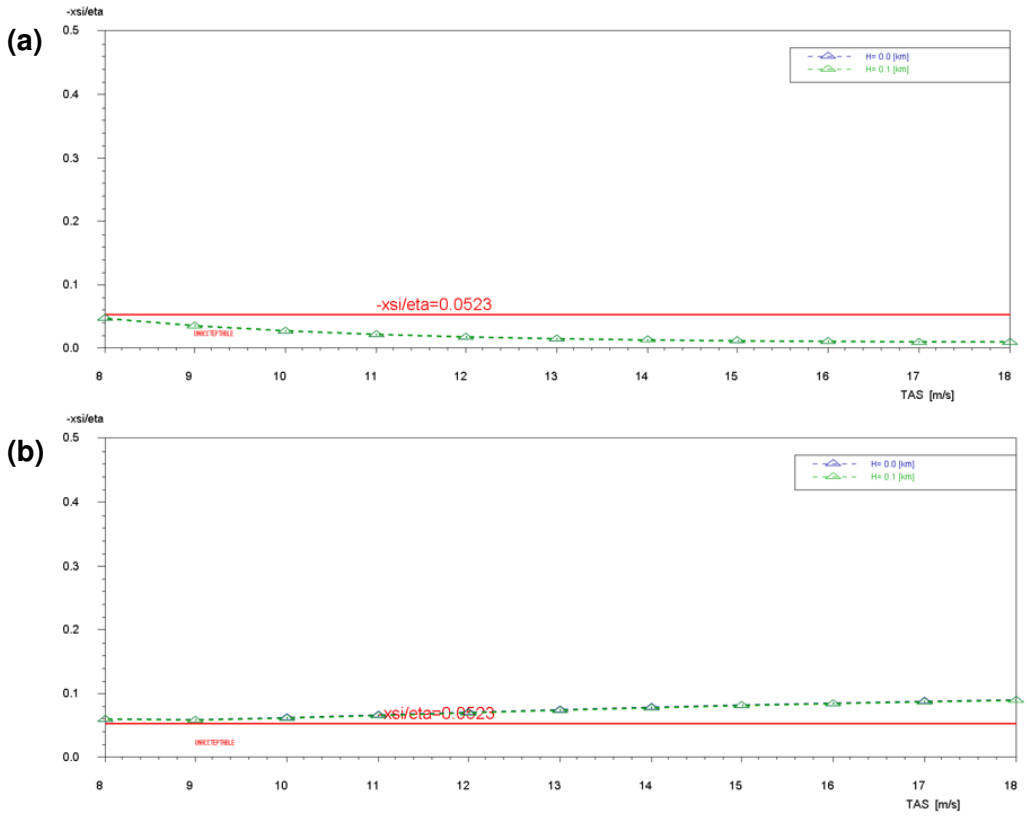

Figure 8 – Dutch roll characteristics comparison a) before optimization b) after optimization [20].

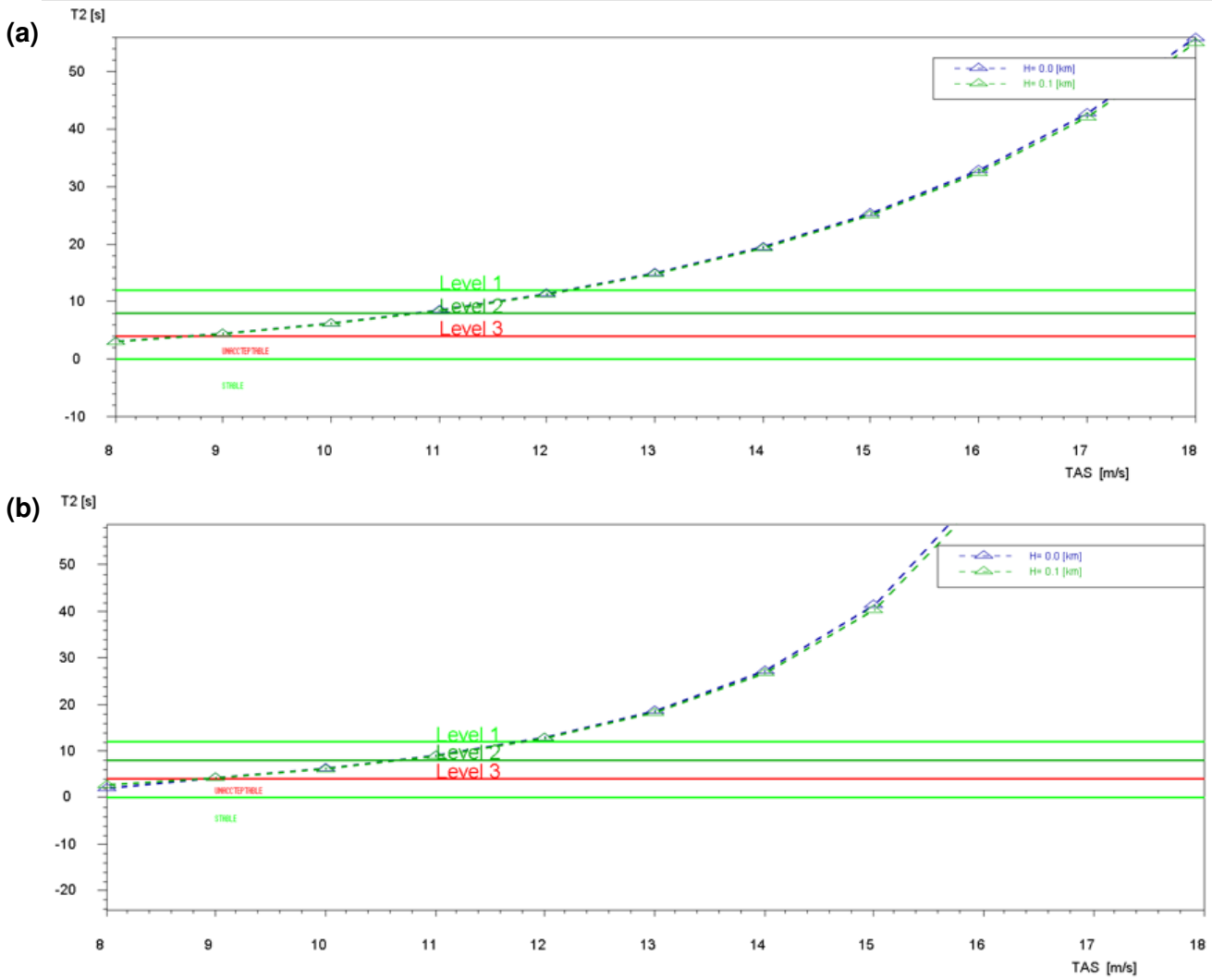

Figure 9 – Spiral characteristics comparison a) before optimization b) after optimization[20].

Before dynamic stability analysis

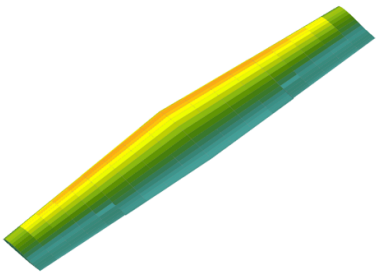

- Lack of vertical surfaces
- No dihedral
- Dutch roll criterion does not met
- Spiral criterion does not met

After dynamic stability analysis

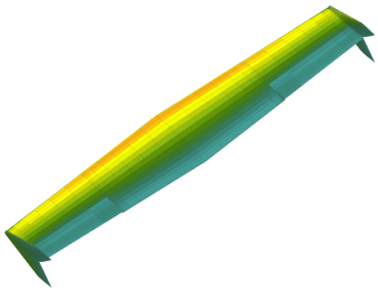

- Vertical surfaces $S = 0.07\ m^2$
- Dihedral angle of 3°
- Dutch roll criterion met
- Improvement in spiral criterion

Figure 10 – Dynamic stability analysis summary.

8. Summary

The optimization successfully increased the UAV's flight time by 23%, mainly through reductions in induced and parasitic drag. The efficiency factor dropped from 1.4 to 1.04, indicating lower induced drag. Dynamic stability was enhanced by adding wingtip vertical surfaces, meeting Dutch roll criteria and reducing induced drag, though parasitic drag increased by 11%.

Key geometry changes included a higher aspect ratio (6 to 6.63) and taper ratio (0.4 to 0.7). Battery capacity decreased by 20%, yet flight time extended by about an hour. Control surface deflection was reduced, further boosting aerodynamic efficiency.

The genetic algorithm proved effective. Future work should include detailed dynamic stability analysis, particularly on low-speed spiral behavior, and real flight tests to validate dynamic responses and endurance in practice.

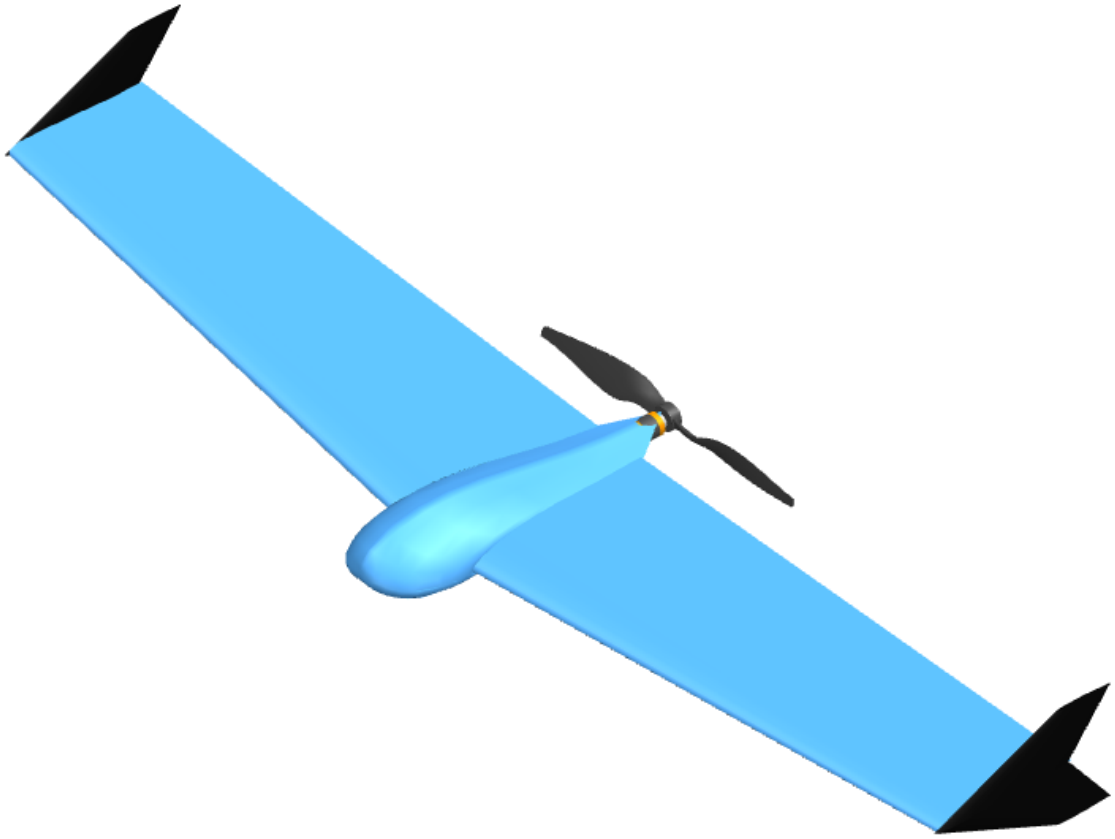

Figure 11 – Final flying wing configuration proposal.

References

[1] M. Arlomandi. Classification of unmanned aerial vehicles. MECH ENG 3016 course note.

[2] Inc. AeroVironment. Small unmanned aircraft systems (uas) | nano drones, 2023. (accessed: 22 August 2024).

[3] Inc. AeroVironment. Raven® small unmanned aircraft system datasheet, 2022. (accessed: 22 August 2024).

[4] Zala e-series uav (unmanned aerial vehicle).

[5] Birdeye 650d. (accessed: 22 August 2024).

[6] Drone open category - applicable requirements to fly from the 1st of january 2024. EASA, 2023.

[7] W. Fiszdon. *Flight Mechanics*. PWN, Warsaw University of Technology., Warszawa, 1952. (in Polish).

[8] S. Staacks, S. Leppler, D. Friedrich, A. Müller, and C. Stampfer. Phyphox: A smartphone-based physics laboratory. *Physikalische Blätter*, 74(1):26–27, 2018.

[9] Skywalker x8 2122mm uav fixed wing, 2024.

[10] J.R.R.A. Martins and A.B. Lambe. Multidisciplinary design optimization: A survey of architectures. *AIAA Journal*, 51(10):2049–2075, 2013.

[11] Matlab documentation, version 9.14 (r2023b). The MathWorks Inc., 2024.

[12] Athena vortex lattice. MIT, 2024.

[13] Global optimization toolbox user's guide, version 9.14 (r2023b). The MathWorks Inc., 2024.

[14] K. Nickel and M. Wohlfahrt. *Tailless Aircraft in Theory and Practice*. Butterworth-Heinemann, Oxford, 1994.

[15] M. Drela. Xfoil – subsonic airfoil development system. MIT.

[16] M.S. Selig. Uiuc airfoil coordinates database, 2024. (accessed: 22 August 2024).

[17] D.P. Raymer. *Aircraft Design: A Conceptual Approach*. American Institute of Aeronautics and Astronautics, Waszyngton, D.C., 1992.

[18] E. Rodríguez-Novillo and A. Sanchez-Carmona. Battery consumption estimation methodology for electric unmanned aerial systems. *The Aeronautical Journal*, 2022.

[19] K. Kubryński and K. Więcko. *Aerodynamic Design and Optimization of Aircraft in a Flying Wing Configuration*. 2022. (in Polish).

[20] T. Goetzendorf-Grabowski, D. Mieszalski, and E. Marcinkiewicz. Stability analysis using sdsa tool. *Prog Aerosp Sci*, 2011.

[21] T. Goetzendorf-Grabowski. Panukl potential solver. Warsaw University of Technology. (accessed: 22 August 2024).

[22] Siemens Digital Industries Software. Nx: Integrated cad, cam, and cae software. `https://www.sw.siemens.com/en-US/nx/`, 2024. (accessed: 22 August 2024).

[23] International Civil Aviation Organization (ICAO). *Annex 8 to the Convention on International Civil Aviation: Airworthiness of Aircraft*. ICAO, 12th edition, 2018.

[24] U.S. Department of Defense. Mil-f-8785c: Military specification: Flying qualities of piloted airplanes, 1980.

[25] European Union Aviation Safety Agency (EASA). Certification specifications for normal, utility, aerobatic, and commuter category aeroplanes (cs-23). `https://www.easa.europa.eu/en/document-library/certification-specifications/cs-23`, 2024. (accessed: 22 August 2024).